

The Rossiter-McLaughlin Effect of the Transiting Exoplanet XO-4b*

Norio NARITA,¹ Teruyuki HIRANO,² Roberto SANCHIS-OJEDA,³ Joshua N. WINN,³
Matthew J. HOLMAN,⁴ Bun'ei SATO,⁵ Wako AOKI,¹ and Motohide TAMURA¹

¹ *National Astronomical Observatory of Japan, 2-21-1 Osawa, Mitaka, Tokyo, 181-8588, Japan*
norio.narita@nao.ac.jp

² *Department of Physics, The University of Tokyo, Tokyo, 113-0033, Japan*

³ *Department of Physics, and Kavli Institute for Astrophysics and Space Research,*
Massachusetts Institute of Technology, Cambridge, MA 02139, USA

⁴ *Harvard-Smithsonian Center for Astrophysics, 60 Garden Street, Cambridge, MA 02138, USA*

⁵ *Global Edge Institute, Tokyo Institute of Technology, 2-12-1 Ookayama, Meguro, Tokyo, 152-8550,*
Japan

(Received 2010 August 23; accepted)

Abstract

We report photometric and radial velocity observations of the XO-4 transiting planetary system, conducted with the FLWO 1.2m telescope and the 8.2m Subaru Telescope. Based on the new light curves, the refined transit ephemeris of XO-4b is $P = 4.1250828 \pm 0.0000040$ days and $T_c [\text{BJD}_{\text{TDB}}] = 2454485.93323 \pm 0.00039$. We measured the Rossiter-McLaughlin effect of XO-4b and estimated the sky-projected angle between the stellar spin axis and the planetary orbital axis to be $\lambda = -46.7^{\circ}_{-6.1^{\circ}}^{+8.1^{\circ}}$. This measurement of λ is less robust than in some other cases because the impact parameter of the transit is small, causing a strong degeneracy between λ and the projected stellar rotational velocity. Nevertheless, our finding of a spin-orbit misalignment suggests that the migration process for XO-4b involved few-body dynamics rather than interaction with a gaseous disk. In addition, our result conforms with the pattern reported by Winn et al. (2010, ApJL, 718, L145) that high obliquities are preferentially found for stars with effective temperatures hotter than 6250 K.

Key words: stars: planetary systems: individual (XO-4) — stars: rotation — techniques: radial velocities — techniques: spectroscopic — techniques: photometric

* Based on data collected at Subaru Telescope, which is operated by the National Astronomical Observatory of Japan.

1. Introduction

Observations of the Rossiter-McLaughlin effect (hereafter the RM effect: Rossiter 1924; McLaughlin 1924; Ohta et al. 2005; Gaudi & Winn 2007; Hirano et al. 2010) for transiting planetary systems enable us to measure the sky-projected angle between the stellar spin axis and the planetary orbital axis (also called the projected spin-orbit angle, or the projected obliquity). Previous measurements of this angle have revealed the existence of well-aligned prograde orbits ($|\lambda| < 10^\circ$; see, e.g., HD 209458b: Queloz et al. 2000; Winn et al. 2005, HD 189733b: Winn et al. 2006), highly-inclined prograde orbits ($10^\circ < |\lambda| < 90^\circ$; XO-3b: Hébrard et al. 2008; Winn et al. 2009b, HD80606b: Moutou et al. 2009; Winn et al. 2009c; Hébrard et al. 2010, WASP-14b: Johnson et al. 2009, CoRoT-1b: Pont et al. 2010), and retrograde orbits ($90^\circ < |\lambda| < 180^\circ$; HAT-P-7b: Narita et al. 2009a; Winn et al. 2009a, WASP-17b: Anderson et al. 2010; Triaud et al. 2010, WASP-33b: Cameron et al. 2010, WASP-8b: Queloz et al. 2010, WASP-15b: Triaud et al. 2010).

The discovery of highly tilted orbits, and retrograde orbits, has been taken as evidence in favor of “few-body” theories for planetary migration, such as planet-planet scattering and subsequent tidal evolution (planet-planet scattering models, e.g., Rasio & Ford 1996; Marzari & Weidenschilling 2002; Nagasawa et al. 2008; Chatterjee et al. 2008), or the Kozai mechanism (Kozai 1962) caused by a distant companion and subsequent tidal evolution (Kozai migration models, e.g., Wu & Murray 2003; Takeda & Rasio 2005; Fabrycky & Tremaine 2007; Wu et al. 2007). In this way, the RM effect has already played an important role for studies of planetary migration processes. Further measurements of the RM effect are important in order to constrain theoretical models by learning the statistical distribution of spin-orbit alignment angles, and by discriminating planetary migration mechanisms for individual planetary systems. For this purpose, we have continued measurements of the RM effect and have also initiated direct imaging observations, with the Subaru 8.2m telescope, of systems with misaligned planets to search for evidence of perturbing stellar companions (e.g., Narita et al. 2007; Narita et al. 2010b).

The subject of this letter is the transiting exoplanet XO-4b, discovered by McCullough et al. (2008) (hereafter MC08). The host star XO-4 is a relatively bright ($V = 10.7$) F5 star, and XO-4b is a giant planet ($M_p = 1.72 M_{\text{Jup}}$, $R_p = 1.34 R_{\text{Jup}}$; MC08) with an orbital period of $P = 4.125$ days. We used the FLWO 1.2m telescope for photometric observations and the Subaru 8.2m telescope for radial velocity (RV) observations. Due to the rapid rotation of XO-4 ($V \sin I_s = 8.8 \pm 0.5 \text{ km s}^{-1}$; MC08), the amplitude of the RM effect for XO-4b was expected to be large. In addition, recently Winn et al. (2010) reported that hot stars ($T_{\text{eff}} > 6250 \text{ K}$) with hot Jupiters tend to have high obliquities. Since XO-4 is a hot star ($T_{\text{eff}} = 6397 \pm 70 \text{ K}$; MC08) with a hot Jupiter, we may use this system as a further test of the proposed pattern. We report our photometric and RV observations in section 2, and describe our analysis procedures

in section 3. We present our results and discussions in section 4. Finally, we summarize the findings of this letter in section 5.

2. Observations

2.1. Light Curves

Photometric observations were conducted with Keplercam on the 1.2m telescope at the Fred Lawrence Whipple Observatory (FLWO) on Mount Hopkins, Arizona. Three partial transits, and one complete transit, were observed with a Sloan Digital Sky Survey (SDSS) z-band filter. The observing dates were UT 2008 October 5 (egress), 2008 October 13 (ingress), 2009 September 8 (ingress), and 2010 February 8 (complete). KeplerCam is equipped with a 4096×4096 CCD, giving a square field of view 23.1' on a side. We used 2×2 binning, giving a scale of 0.68" per binned pixel, a readout and setup time of 11 s, and a typical readout noise of 7 e⁻ per binned pixel. The cadence was typically 2 min for the observation on UT 2010 February 8, and about 50 s for the other observations. Standard IRAF¹ procedures were applied to the observed frames for bias subtraction, flat-field division, and aperture photometry. The flux of XO-4 was divided by the sum of the fluxes of 11 nearby reference stars in the field of view. To account for systematic effects due to differential airmass extinction and imperfect flat-fielding, we corrected the baseline of the observed flux as a function of time and airmass. Photometric uncertainties were temporarily set equal to the standard deviation of the out-of-transit relative flux on that night. As explained in subsection 3.1, we subsequently rescaled these uncertainties to account for time-correlated noise. The upper panel of figure 1 shows the composite transit light curves.

2.2. Radial Velocities

We observed XO-4 on UT 2010 January 14, 2010 January 15, 2010 February 4, and 2010 May 17 with the High Dispersion Spectrograph (HDS: Noguchi et al. 2002) on the 8.2m Subaru Telescope at Mauna Kea, Hawaii. The observations on 2010 January 15 covered a full transit of XO-4b. We employed the standard I2a setup of the HDS, covering the wavelength range 4940 Å < λ < 6180 Å and a slit width of 0".4, corresponding to a spectral resolution of about 90000. We used the iodine gas absorption cell for precise differential RV measurements. The exposure times were 15–20 min, yielding a typical signal-to-noise ratio (SNR) of approximately 80–100 per pixel. We processed the observed frames with standard IRAF procedures and extracted one-dimensional spectra. We computed relative RVs following the algorithm of Butler et al. (1996) and Sato et al. (2002). We estimated the internal error of each RV based on the scatter among the RV solutions from ~4 Å segments of each spectrum. The typical internal errors were

¹ The Image Reduction and Analysis Facility (IRAF) is distributed by the U.S. National Optical Astronomy Observatories, which are operated by the Association of Universities for Research in Astronomy, Inc., under cooperative agreement with the National Science Foundation.

9–15 m s⁻¹. As was the case for TrES-4 (Narita et al. 2010a), the internal errors are larger than some other cases of spectra with a similar SNR due to the star’s broad absorption features. The observed RVs and internal errors are given in table 1. We note that we adopt BJD_{TDB}, the Barycentric Julian Date in the Barycentric Dynamical Time standard, for all time stamps in this letter, as advocated by Eastman et al. (2010).

3. Analyses

3.1. Refined Transit Ephemeris

First we fitted the FLWO transit light curves in order to determine appropriate data weights for our subsequent analysis, and to refine the transit ephemeris of XO-4b. We used the analytic formula for transit light curves given by Ohta et al. (2009). The free parameters were the midtransit time T_c for each transit, the ratio of radii of the planet and star R_p/R_s , the orbital inclination i , and the orbital distance in units of the stellar radius a/R_s . We here adopted the orbital period $P = 4.12502$ days, the origin of mid-transit time of XO-4b $T_c(0) = 2454485.93295 \pm 0.00040$ in BJD_{TDB}, the stellar mass $M_s = 1.32 M_\odot$ reported by MC08. We held fixed one of quadratic limb-darkening coefficients u_1 at the value 0.13, based on tables of Claret (2004), and allowed u_2 to be a free parameter.

We determined the optimal parameter values by minimizing the χ^2 statistic,

$$\chi^2 = \sum_i \left[\frac{f_{i,\text{obs}} - f_{i,\text{calc}}}{\sigma_i} \right]^2, \quad (1)$$

using the AMOEBA algorithm (Press et al. 1992). In this equation, $f_{i,\text{obs}}$ are the relative flux data points, and $f_{i,\text{calc}}$ are the values calculated based on the analytic formulae and a particular choice of model parameters.

We then computed the residuals for each dataset, and averaged the residuals into M bins of N points. We calculated the standard deviation of the binned data, $\sigma_{N,\text{obs}}$ and

$$\sigma_{N,\text{ideal}} = \frac{\sigma_1}{\sqrt{N}} \sqrt{\frac{M}{M-1}}, \quad (2)$$

where σ_1 is the standard deviation of the residuals for each dataset. To account for increased uncertainties due to time-correlated noise (so-called red noise; see e.g., Gillon et al. 2006; Winn et al. 2008), we computed a red noise factor $\beta = \sigma_{N,\text{obs}}/\sigma_{N,\text{ideal}}$ for various N (corresponding to 10-20 min), and multiplied the photometric uncertainties of each dataset by the maximum value of β . We estimated 1σ uncertainties of free parameters based on the criterion $\Delta\chi^2 = 1.0$. Table 2 summarizes the rms, the red noise factor, and the mid-transit time of each transit light curve. One important result is that $i = 90^\circ$ is allowed within the 1σ level. This was problematic for subsequent RM modeling, because the two key parameters describing the RM effect (λ and $V \sin I_s$, see below) are strongly degenerate when $i = 90^\circ$.

We then fitted all the observed mid-transit times with a linear function

$$T_c(E) = EP + T_c(0), \quad (3)$$

where E is an integer, in order to refine the orbital period of XO-4b. We note that we added 0.00075 to the value of $T_c(0)$ reported by MC08 to convert the time standard from HJD_{UTC} (the Heliocentric Julian Date in the Coordinated Universal Time) to BJD_{TDB} (Eastman et al. 2010).

The refined transit ephemeris for XO-4b is $P = 4.1250828 \pm 0.0000040$ days and $T_c(0) = 2454485.93323 \pm 0.00039$ in the BJD_{TDB} system. We note that the linear fit gave $\chi^2 = 6.99$ and all O-C residuals were within 1.5σ uncertainties of $T_c(E)$. The uncertainty in the predicted time of the transit of UT 2010 January 15 (the night of our RM measurement) is about 1 min, which is small enough to be of no concern for our RM modeling.

3.2. RM Model and Joint Fitting

To describe the RM effect of XO-4b, we derived a formula based on the procedure described in Winn et al. (2005), Narita et al. (2009b), and Hirano et al. (2010). We assumed a rotational broadening kernel of $V \sin I_s = 8.8 \text{ km s}^{-1}$ (MC08) and the quadratic limb-darkening parameters $u_1 = 0.35$ and $u_2 = 0.35$ for the iodine absorption band based on the tables of Claret (2004). The derived formula was

$$\Delta v = -f v_p \left[1.6159 - 0.83778 \left(\frac{v_p}{V \sin I_s} \right)^2 \right]. \quad (4)$$

In this formula, Δv is the anomalous radial velocity due to the RM effect, f is the loss of light, and v_p is the subplanet velocity (the radial component of the stellar rotation velocity at the position being hidden by the planet).

We simultaneously fitted the Subaru RVs and the FLWO light curves. We fixed P and $T_c(0)$ at the central values reported above. We did not fit the RVs reported by MC08 because the errors of the MC08 RVs are much larger than those of the Subaru RVs. Thus, those data have little impact on the results. In addition to the free parameters for the photometric data, we added free parameters for the radial velocity semiamplitude K , the sky-projected angle between the stellar spin axis and the planetary orbital axis λ , the sky-projected stellar rotational velocity $V \sin I_s$, and the overall velocity offset of the Subaru dataset v_1 . Note that we fixed the eccentricity e to zero, and the argument of periastron ω was not considered. (When e and ω were included as free parameters, the eccentricity was found to be consistent with zero within 1σ .) The χ^2 statistic for the joint fit was

$$\chi^2 = \sum_i \left[\frac{f_{i,\text{obs}} - f_{i,\text{calc}}}{\sigma_i} \right]^2 + \sum_j \left[\frac{v_{j,\text{obs}} - v_{j,\text{calc}}}{\sigma_j} \right]^2 + \left[\frac{V \sin I_s - 8.8}{0.5} \right]^2,$$

where $v_{j,\text{obs}}$ were the observed RVs and $v_{j,\text{calc}}$ were RVs calculated based on the Keplerian motion and on the RM formula given above. The last term was an *a priori* constraint on $V \sin I_s$ to require consistency with the value reported by MC08 within its uncertainty. This term was necessary to obtain a meaningful conclusion about λ , as a consequence of the low

impact parameter (near-90° inclination) of the transit (see subsection 3.1.).

4. Results and Discussion

The lower panel of figure 1 shows the RVs around the transit phase, along with the best-fitting model (the solid line). For reference, we have also plotted a model RV curve under the assumption of perfect spin-orbit alignment ($\lambda = 0^\circ$, the dotted line). We found small asymmetry of the RM anomaly with respect to the midtransit time, suggesting that the transit is not exactly equatorial and that there is a significant spin-orbit misalignment.

Figure 2 plots the full RV dataset in BJD_{TDB} (left panel) and in phase (right panel). No significant long term trend was observed in the residuals. Table 3 summarizes the optimal values and uncertainties for the system parameters. As shown in table 3, the free parameters other than the RM-related parameters (λ and $V \sin I_s$) are consistent with those reported previously. For the RM-related parameters, we found $\lambda = -46.7^\circ_{-6.1^\circ}^{+8.1^\circ}$ and $V \sin I_s = 8.9 \pm 0.5 \text{ km s}^{-1}$. We also computed the 3σ confidence level of λ by $\Delta\chi^2 = 9.0$ and found $\lambda = -46.7^\circ_{-14.8^\circ}^{+41.7^\circ}$. Figure 3 shows a χ^2 contour map in λ - $V \sin I_s$ space. The solid lines represent contours for $\Delta\chi^2 = 1.0$, $\Delta\chi^2 = 4.0$, and $\Delta\chi^2 = 9.0$ from the inside to the outside. The orbital axis of XO-4b appears to be tilted relative to the rotational axis of XO-4 in sky projection at about the 3σ level.

It should be noted that the confidence with which λ is found to be nonzero depends critically on the *a priori* constraint that we applied on $V \sin I_s$. This is because when the transit impact parameter is small (or equivalently when the orbital inclination is near 90°), there is a strong degeneracy between $V \sin I_s$ and λ . In such cases, the RV data alone are only able to provide good constraints on the quantity $V \sin I_s \cos \lambda$, while $V \sin I_s \sin \lambda$ is poorly constrained. When we tried the joint fitting without the *a priori* constraint, we found $V \sin I_s \cos \lambda = 8.4 \pm 1.1 \text{ km s}^{-1}$, $V \sin I_s = 10.0_{-2.2}^{+72.0} \text{ km s}^{-1}$, $\lambda = -54.6^\circ_{-35.4^\circ}^{+19.2^\circ}$, and $i = 89.1^\circ \pm 0.9^\circ$ at the 1σ level. In this case the confidence in the spin-orbit misalignment was lowered, and values of $V \sin I_s$ differing strongly from that reported by MC08 were allowed within 1σ .

As long as the spectroscopic determination of $V \sin I_s$ is valid, our result of a strong spin-orbit misalignment is secure. However, in order to make the result more robust, and less dependent on the spectroscopic determination of $V \sin I_s$, it would be necessary to obtain a more stringent constraint on the inclination i . The most straightforward way to do so would be to obtain a more precise light curve. It is difficult to observe complete transits from the ground, because of the comparatively long orbital period and long duration of the transits. However, the system is in the continuous viewing zone of the Hubble Space Telescope (*HST*), as noted by MC08. A complete transit light curve based on *HST* observations is therefore the highest priority for pinning down the spin-orbit angle.

From a theoretical point of view, it is interesting that the planetary orbit is highly tilted, given that the orbital eccentricity of XO-4b is consistent with zero at this point in time. However, the current bounds on the orbital eccentricity are coarse; improving the determination

of this parameter is also a priority for future work.

Recently, Winn et al. (2010) pointed out that hot Jupiters around relatively hot ($T_{\text{eff}} > 6250$ K) stars preferentially have tilted orbits. According to the empirical rule, XO-4, which has an effective temperature of $T_{\text{eff}} = 6397 \pm 70$ K (MC08), would have a tilted orbit. Our results agree with this prediction.

In addition, Schlaufman (2010) has recently sought evidence for spin-orbit misalignments along the line of sight, based on the comparison of the measured $V \sin I_S$ and the plausible range of rotation velocities for a star of the given mass, radius, and age. He argued that if a value $\Theta \equiv (V \sin I_{s,\text{sim}} - V \sin I_{s,\text{obs}}) / \sqrt{\sigma_{\text{sim}}^2 + \sigma_{\text{obs}}^2}$ is larger than 2.9 (a threshold based on the SPOCS catalog: Valenti & Fischer 2005), the stellar rotational axis is very likely to be inclined with respect to the line of sight. For a transiting planet host, this would imply a spin-orbit misalignment. (He also found that hot stars were more likely to have high obliquities, although he phrased the correlation in terms of stellar mass rather than effective temperature.) For XO-4, the value is $\Theta = 2.61$, which is only just below the (somewhat arbitrary) threshold of 2.9. This suggests that XO-4 has a smaller projected rotational velocity than expected, and can be taken as supporting evidence for a spin-orbit misalignment in the XO-4 system.

5. Summary

We conducted photometric transit observations with the FLWO 1.2m telescope, and RV observations (including an RM measurement) with the 8.2m Subaru Telescope, for the exoplanet XO-4b. We refined the transit ephemeris for XO-4b based on the new transit light curves, and modeled the RM effect of XO-4b by jointly fitting the photometry and RVs. In conjunction with the previous spectroscopic estimate of the projected stellar rotational velocity $V \sin I_s$, we found evidence for spin-orbit misalignment in this system. In this case the RM data do not provide an strong independent constraint on $V \sin I_s$, because of the low impact parameter of the transit. To complement the RM measurement in this system, a more stringent constraint on the orbital inclination would be useful to break the fitting degeneracy between λ and $V \sin I_s$.

The spin-orbit misalignment of XO-4b suggests that this planet migrated through a mechanism that excited its orbital inclination, although the eccentricity of XO-4b seemed to be quite low. Furthermore, the spin-orbit misalignment of XO-4b is consistent with the findings by Winn et al. (2010) and Schlaufman (2010) that hot stars with hot Jupiters have high obliquities. Further follow-up observations to determine a more accurate spin-orbit alignment angle in this system would be still interesting.

This letter is based on data collected at Subaru Telescope, which is operated by the National Astronomical Observatory of Japan. We acknowledge the support for our Subaru HDS observations by Akito Tajitsu, a support scientist for the Subaru HDS. The data analysis was in part carried out on common use data analysis computer system at the Astronomy Data

Center, ADC, of the National Astronomical Observatory of Japan. N.N. and T.H. are supported by a Japan Society for Promotion of Science (JSPS) Fellowship for Research (PD: 20-8141, DC1: 22-5935). R.S. is funded by Caja de Ahorros y Pensiones de Barcelona, "la Caixa", under the Fellowship Program to extend graduate studies in the United States. We gratefully acknowledge support from the NASA Origins program through award NNX09AD36G (to J.N.W.) and NNX09AB33G (to M.J.H. and J.N.W.), as well as the MIT Class of 1942. KeplerCam was developed with partial support from the Kepler mission under NASA Cooperative Agreement NCC2-1390 (PI: D. Latham). M.T. is supported by the Ministry of Education, Science, Sports and Culture, Grant-in-Aid for Specially Promoted Research, 22000005. We wish to acknowledge the very significant cultural role and reverence that the summit of Mauna Kea has always had within the indigenous people in Hawai'i.

References

- Anderson, D. R., et al. 2010, *ApJ*, 709, 159
- Butler, R. P., Marcy, G. W., Williams, E., McCarthy, C., Dosanjuh, P., & Vogt, S. S. 1996, *PASP*, 108, 500
- Cameron, A. C., et al. 2010, *MNRAS*, 882
- Chatterjee, S., Ford, E. B., Matsumura, S., & Rasio, F. A. 2008, *ApJ*, 686, 580
- Claret, A. 2004, *A&A*, 428, 1001
- Eastman, J., Siverd, R., & Gaudi, B. S. 2010, *ArXiv e-prints*
- Fabrycky, D., & Tremaine, S. 2007, *ApJ*, 669, 1298
- Gaudi, B. S., & Winn, J. N. 2007, *ApJ*, 655, 550
- Gillon, M., Pont, F., Moutou, C., Bouchy, F., Courbin, F., Sohy, S., & Magain, P. 2006, *A&A*, 459, 249
- Hébrard, G., et al. 2008, *A&A*, 488, 763
- Hébrard, G., et al. 2010, *A&A*, 516, A95
- Hirano, T., Suto, Y., Taruya, A., Narita, N., Sato, B., Johnson, J. A., & Winn, J. N. 2010, *ApJ*, 709, 458
- Johnson, J. A., Winn, J. N., Albrecht, S., Howard, A. W., Marcy, G. W., & Gazak, J. Z. 2009, *PASP*, 121, 1104
- Kozai, Y. 1962, *AJ*, 67, 591
- Marzari, F., & Weidenschilling, S. J. 2002, *Icarus*, 156, 570
- McCullough, P. R., et al. 2008, *ArXiv e-prints (MC08)*
- McLaughlin, D. B. 1924, *ApJ*, 60, 22
- Moutou, C., et al. 2009, *A&A*, 498, L5
- Nagasawa, M., Ida, S., & Bessho, T. 2008, *ApJ*, 678, 498
- Narita, N., Sato, B., Hirano, T., & Tamura, M. 2009a, *PASJ*, 61, L35
- Narita, N., Sato, B., Hirano, T., Winn, J. N., Aoki, W., & Tamura, M. 2010a, *PASJ*, 62, 653
- Narita, N., Sato, B., Ohshima, O., & Winn, J. N. 2008, *PASJ*, 60, L1

Narita, N., et al. 2007, PASJ, 59, 763
Narita, N., et al. 2009b, PASJ, 61, 991
Narita, N., et al. 2010b, PASJ, 62, 779
Noguchi, K., et al. 2002, PASJ, 54, 855
Ohta, Y., Taruya, A., & Suto, Y. 2005, ApJ, 622, 1118
Ohta, Y., Taruya, A., & Suto, Y. 2009, ApJ, 690, 1
Pont, F., et al. 2010, MNRAS, 402, L1
Press, W. H., Teukolsky, S. A., Vetterling, W. T., & Flannery, B. P. 1992, Numerical recipes in C.
The art of scientific computing (Cambridge: University Press, —c1992, 2nd ed.)
Queloz, D., Eggenberger, A., Mayor, M., Perrier, C., Beuzit, J. L., Naef, D., Sivan, J. P., & Udry, S.
2000, A&A, 359, L13
Queloz, D., et al. 2010, A&A, 517, L1
Rasio, F. A., & Ford, E. B. 1996, Science, 274, 954
Rossiter, R. A. 1924, ApJ, 60, 15
Sato, B., Kambe, E., Takeda, Y., Izumiura, H., & Ando, H. 2002, PASJ, 54, 873
Schlaufman, K. C. 2010, ApJ, 719, 602
Takeda, G., & Rasio, F. A. 2005, ApJ, 627, 1001
Triaud, A. H. M. J., et al. 2010, ArXiv e-prints
Valenti, J. A., & Fischer, D. A. 2005, ApJS, 159, 141
Winn, J. N., Fabrycky, D., Albrecht, S., & Johnson, J. A. 2010, ApJL, 718, L145
Winn, J. N., Johnson, J. A., Albrecht, S., Howard, A. W., Marcy, G. W., Crossfield, I. J., & Holman,
M. J. 2009a, ApJL, 703, L99
Winn, J. N., et al. 2005, ApJ, 631, 1215
Winn, J. N., et al. 2006, ApJL, 653, L69
Winn, J. N., et al. 2008, ApJ, 683, 1076
Winn, J. N., et al. 2009b, ApJ, 700, 302
Winn, J. N., et al. 2009c, ApJ, 703, 2091
Wu, Y., & Murray, N. 2003, ApJ, 589, 605
Wu, Y., Murray, N. W., & Ramsahai, J. M. 2007, ApJ, 670, 820

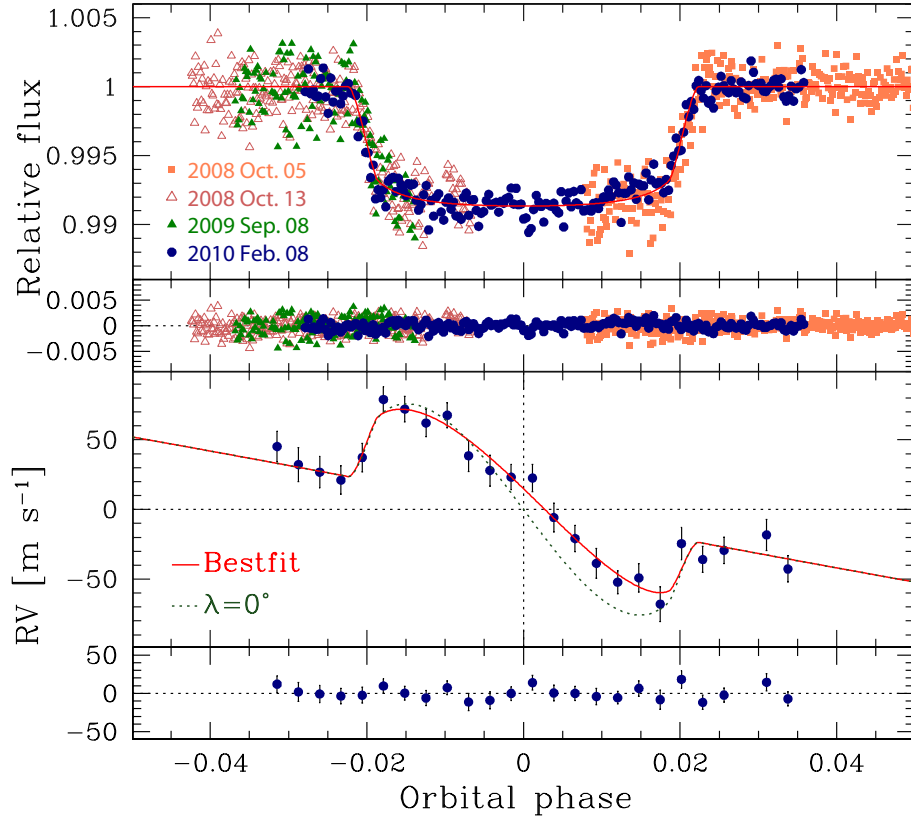


Fig. 1. Top panel: Phased transit light curves taken with the FLWO 1.2m telescope. Four different epoch data are combined. The solid line represents the best-fit curve based on the optimal free parameters listed in table 3. Second panel: Residuals of the photometric data from the best-fit model. Third panel: Subaru radial velocities and the best-fit curve (the solid line) as well as a model curve which assumed $\lambda = 0^\circ$ (the dotted line). Bottom panel: Residuals of radial velocities from the best-fit model.

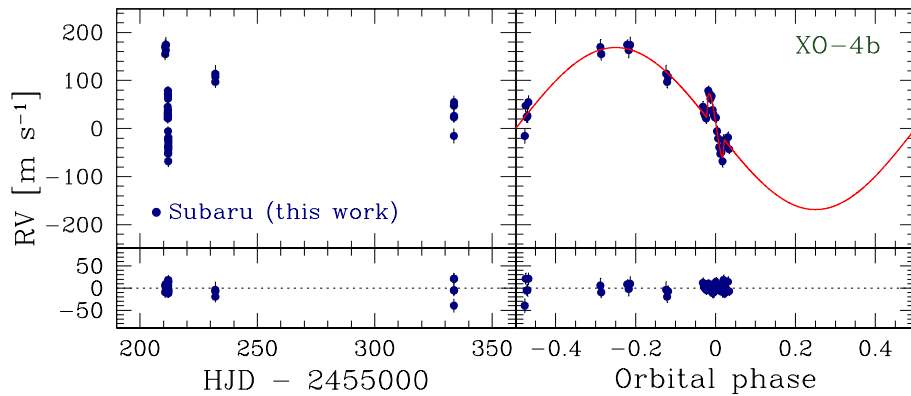


Fig. 2. Upper panels: Subaru radial velocities in BJD_{TDB} (left panel) and in phase (right panel). Lower panels: Residuals from the best-fit model. No significant long term trend is apparent.

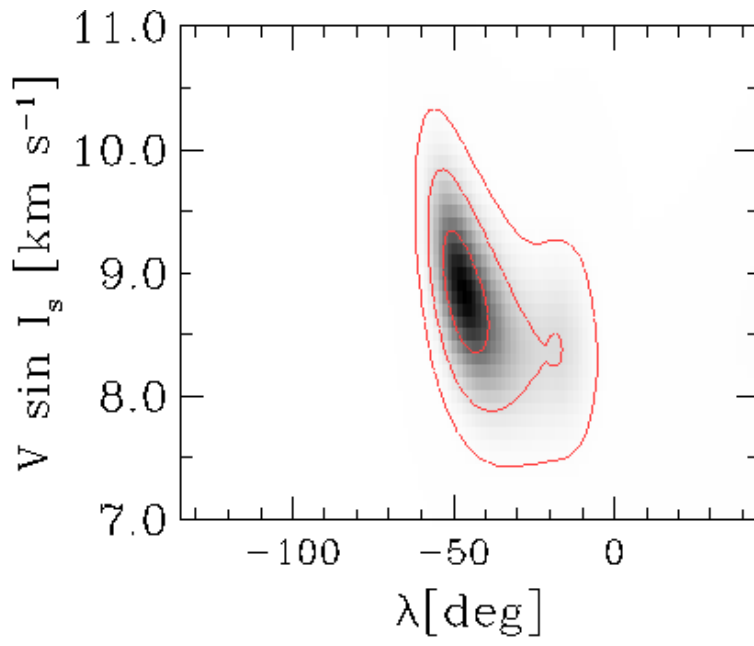


Fig. 3. A χ^2 contour map in λ - $V \sin I_s$ space. The solid lines represent contours for $\Delta\chi^2 = 1.0$, $\Delta\chi^2 = 4.0$, and $\Delta\chi^2 = 9.0$ from the inside to the outside.

Table 1. Radial velocities obtained with the Subaru/HDS.

Time [BJD _{TDB}]	Value [m s ⁻¹]	Error [m s ⁻¹]
2455210.75952	169.41	16.13
2455210.76897	154.86	12.81
2455211.03700	174.33	10.06
2455211.05170	163.09	16.51
2455211.06638	173.97	16.29
2455211.81802	45.11	10.91
2455211.82923	32.15	12.19
2455211.84044	26.67	11.31
2455211.85165	21.03	10.25
2455211.86285	37.17	10.35
2455211.87405	78.81	9.42
2455211.88526	72.01	9.11
2455211.89646	61.92	9.83
2455211.90768	67.59	9.19
2455211.91890	38.45	11.15
2455211.93011	27.91	11.16
2455211.94132	23.14	9.01
2455211.95255	22.51	9.83
2455211.96377	-5.80	10.34
2455211.97497	-20.92	9.45
2455211.98619	-38.70	10.70
2455211.99740	-52.24	8.29
2455212.00861	-49.20	10.16
2455212.01982	-68.05	12.48
2455212.03102	-24.63	11.57
2455212.04223	-35.98	9.33
2455212.05343	-29.42	9.41
2455212.07586	-18.34	11.22
2455212.08708	-42.78	9.52
2455232.06436	114.02	18.42
2455232.07383	97.09	13.09
2455232.08330	107.35	12.66
2455333.73171	-15.49	15.33
2455333.74176	47.77	12.39
2455333.75088	23.27	11.23
2455333.76001	26.43	13.70
2455333.76915	12.67	13.64

Table 2. Summary of the XO-4 transit light curves.

UT Date	Epoch	RMS	Red noise factor	Mid-transit time	Note
	E	$10^4\sigma$	β	BJD_{TDB}	
2008 Jan. 20	0	—	—	$2454485.93295 \pm 0.00040$	MC08
2008 Oct. 05	63	12.7	1.293	$2454745.81494 \pm 0.00105$	Egress
2008 Oct. 13	64	15.4	1.497	$2454749.93969 \pm 0.00114$	Ingress
2009 Sep. 08	144	17.2	1.002	$2455079.94672 \pm 0.00110$	Ingress
2010 Feb. 08	182	8.2	1.807	$2455236.69753 \pm 0.00065$	Complete

Table 3. System parameters of XO-4 derived from the joint fitting.

Parameter	Value	Uncertainty	Note
Adopted parameters			
P [days]	4.1250828	± 0.0000040	this work
$T_c(0)$ [BJD _{TDB}]	2454485.93323	± 0.00039	this work
M_s [M_\odot]	1.32	± 0.02	MC08
$V \sin I_s$ [km s ⁻¹]	8.8	± 0.5	MC08
u_1	0.13	—	Claret (2004)
e	0	—	assumed
Best-fit parameters with the <i>a priori</i> constraint			
K [m s ⁻¹]	168.6	± 6.2	
$V \sin I_s$ [km s ⁻¹]	8.9	± 0.5	
λ [°]	-46.7	$^{+8.1}_{-6.1}$	$^{+41.7}_{-14.8}$ (3σ)
a/R_s	7.68	± 0.11	
R_p/R_s	0.0881	± 0.0007	
i [°]	88.8	± 0.6	
u_2	0.35	± 0.11	
v_1 [m s ⁻¹]	-0.1	± 2.9	
rms [m s ⁻¹]	11.50	—	
χ^2/ν (RV)	31.63/37	—	
χ^2/ν (LC)	487.22/906	—	
Derived planet parameters			
M_p [M_{Jup}]	1.78	± 0.08	this work
R_p [R_{Jup}]	1.33	± 0.05	this work
Comparison with previous literature			
K [m s ⁻¹]	163	± 16	MC08
a/R_s	7.7	± 0.2	MC08
R_p/R_s	0.089	± 0.001	MC08
i [°]	88.7	± 1.1	MC08
M_p [M_{Jup}]	1.72	± 0.20	MC08
R_p [R_{Jup}]	1.34	± 0.048	MC08
u_2	0.36	—	Claret (2004)